Engineering Considerations for the Development of Disk Spring Stacks for Vibration Isolation

Coned disk springs exhibit significant nonlinear properties including the quasi-zero stiffness regimes that are useful in isolating equipment at the lower frequency vibrations. However, the stroke of a single disk spring is too low for most applications, and thus springs must be stacked to increase the deflection. Development of such isolator stacks then becomes critical for practical uses. The goal of this article is to identify challenges and engineering considerations in developing such stacks within the practical constraints. For instance, how to appropriately contain the stack without affecting the low-frequency isolation performance. Three designs are analyzed: a retaining ring design, tube and shaft design, and zero Poison's ratio sleeve design. Disk spring stack protypes with each containment method are built, and force-deflection curves are measured and compared with the standalone stacks. Under quasi-static compression testing, each containment method has minimal effect on the standalone stack force-deflection curve. However, significant advantages of certain methods are found including lateral stability, lateral strength, and degrees of freedom. Lastly, advantages, disadvantages, and appropriate applications for each containment method are summarized, and are demonstrated. Salient contribution of this work is the identification of engineering considerations that would lead to robust or versatile containment designs. This has been overlooked in the scientific literature as the stack containment methods are found to be important in the design of isolation devices.

Primary subject classification: vibration isolation; Secondary subject classification: quasi-zero stiffness

1 INTRODUCTION

Quasi-zero stiffness (QZS) is a well-known vibration isolation concept in the scientific literature[1-18] to isolate objects from low frequency vibrations without sacrificing load bearing capability. A multi-staged isolator must have high stiffness at lower deflections for load bearing capability and almost zero stiffness at higher deflections, leading to the high-static-low-dynamic-stiffness (HSLDS) property[1]. Many QZS structures have been proposed, and some of these are mechanical linkages composed of different springs, bi-stable elements, cams, and rollers in order to create the desired nonlinear stiffness in a particular direction[2-6]. Pneumatic and magnetic components have also been utilized to improve upon the limitations of purely mechanical devices[7-9]. The way in which many of these mechanisms achieve a QZS effect is by combining a positive stiffness element with a negative stiffness element. Then with proper design, the net stiffness becomes almost zero at a certain deflection. For example, a vertical spring combined with two lateral springs is the most common implementation of this strategy[10-11]. Yet another common example of negative stiffness elements is the coned disk spring element that is commercially available and could be combined with positive vertical stiffness elements to make QZS isolators[12-15].

However, little work has been done on the engineering development aspects and practical implementation of the concepts. Thus, the major goals of this paper are to demonstrate the effectiveness of disk spring QZS isolators (such as in terms of compactness), and to develop engineering approaches to assemble and contain the isolator stacks for practical applications.

2 PROBLEM FORMULATION

While the previous function of disk springs in QZS isolators has been the negative stiffness element, this article focuses on designing disk springs as a standalone zero stiffness component. The deflection of a single disk spring is small, and stacking disk springs in series theoretically increases the deflection while maintaining the same QZS force. Such a design can therefore overcome the small working range limitation of many QZS isolators. The concept to use a stack for vibration isolation was also considered by Valeev et al[16-17]. Some basic design calculations were performed, but no fabrication method and experimental data were presented. In order to demonstrate the concept, we propose a compact stack design that can be easily manufactured and customized, and we conduct static and dynamic testing to prove the feasibility.

Another challenge of disk spring stack design is the presence of multiple nonlinear elements in series. Force-deflection models of individual disk springs have been developed, but the ways in which those models can be extended to a stack are limited. For instance, if a stack has n disk springs and every spring is equivalent, it may be assumed that the deflections of the springs are always equal. Then, an overall force-deflection equation for the stack can be approximated by substituting δ/n for δ in the force-deflection relationship for a single disk spring, where δ is the spring deflection. This assumption is used in the existing disc spring stack literature, making it easy to develop a stack equation from the single spring equation[16-18]. It is important to determine the validity of this assumption through experiments. Accordingly, the specific objectives of this article are as follows: 1. propose a novel disk spring stack (including the insertion of rigid spacers between the springs) for use as a quasi-zero stiffness vibration isolator, 2. determine the important static characteristics of disk spring stacks through experimental and computational studies, and 3. assess the feasibility and transmissibility of a disk spring stack QZS isolator through base excitation experiments.

3 TYPICAL NONLINEAR CHARACTERISTICS OF CONED DISKS

A single disk spring geometry is completely defined by its height, thickness, inner diameter and outer diameter as given in Fig. 1a. The force-deflection relationship which accounts for friction at the upper and lower edge contacts is given by the following analytical solution[19]:

$$P(\delta) = \frac{\frac{E\delta\pi}{a^2}\left(\frac{\alpha}{\alpha-1}\right)^2\left[(h-\delta)\left(h-\frac{\delta}{2}\right)\left(\frac{\alpha+1}{\alpha-1}-\frac{2}{\ln(\alpha)}\right)\tau+\frac{\tau^3}{6}\ln\alpha\right]}{1-\left[\frac{[a\mu_a-b\mu_b-c(\mu_a-\mu_b)](h-\delta)}{(a-b)^2}+\frac{\tau(\mu_a+\mu_b)}{2(a-b)}\right]\mathrm{sgn}(\dot{\delta})} \tag{1}$$

where P is the force, δ is the deflection, a is the outer radius, b is the inner radius, $\alpha = a/b$, E is Young's modulus, and c is the point about which the disk spring cross section rotates:

$$c = a\left(\frac{v}{1-v}\right)\left(\frac{\alpha^{v-1}-1}{1-\alpha^v}\right) \tag{2}$$

Fundamental assumptions used to derive this equation are (i) the loads are evenly distributed around the disk spring circumference, (ii) the disk spring angular rotation is small and small angle approximation can be used, (iii) radial stresses are negligible, (iv) the cross section does not distort, and (v) the friction coefficients of upper and lower surfaces are equal. The coefficients of friction at the lower and upper surfaces (μ_a and μ_b) were assumed to be equal for this study. The second term in the denominator accounts for the hysteresis due to edge friction between disk spring and upper and lower contacts.

Assuming δ is positive downward as shown, sgn($\dot{\delta}$) is 1 when the spring is being compressed and -1 when the spring is being relaxed. As a result, the force during compression is higher than the force during relaxation, and hysteresis is created.

The nonlinear force-deflection characteristics of disk springs depend significantly on the height to thickness ratio, h/τ. Typical force-deflection curves for a few h/τ ratios are plotted in Fig. 1b, and this is a well-known aspect of the commercially available conical disk springs[20]. When the h/τ ratio is 1.41, the stiffness is zero at the deflection midpoint. Therefore, this specific geometry can be used to achieve the QZS behavior with a single component, avoiding the need to correctly balance negative and positive stiffness components in previous QZS isolators. A commercially available disk spring with h/τ ratio very close to 1.41 is chosen for this study. It is made from steel, has the nominal geometry given in Table 1, and is assumed to have a Young's modulus of 200 GPa.

Friction has been recognized to be an important factor in the design and performance of QZS isolators[18-19]. It may never be completely eliminated in mechanical devices yet the majority of QZS models do not often account for friction or other coulomb-type damping. The influence of friction is examined by using Eqn. (1) to plot the loading direction force-deflection curves of the commercial spring. Friction in coned disk springs introduces not only force-deflection hysteresis but a change in stiffness in the QZS region. As seen in Fig. 2(a-b), when the edge friction coefficient is mathematically zero, the slope is zero at the midpoint ($\delta = h$). As the edge friction increases, the slope at the midpoint becomes more negative. Typical edge friction coefficients for steel-steel contacts are in the range of 0.4-0.8. The minimum slope varies from -6 to -15 N/mm within the range. However, the overall effect of friction on the force-deflection behavior is relatively insignificant compared to the effect of h/τ ratio. Therefore, we conclude that while friction may be an interesting parameter to exploit in optimizing damping performance, a tighter control of the h/τ ratio is more important for achieving zero stiffness.

4 ENGINEERING DESIGN CONSIDERATIONS OF DISK SPRING STACK

The working range of the QZS region is small as observed from Fig. 2a. A stacked design is necessary to increase the deflection for practical applications. The basic components and design of the proposed disk spring stack are seen in Fig. 3. Multiple springs are separated by rigid inner and outer spacers, and the primary functions of these spacers, by design, are as follows. First, spacers allow each spring to be compressed past the flat position to the fully inverted position without interference between adjacent springs. This allows the stroke to be doubled compared to a stack without spacers and eliminates the need for a very stiff stopper effect that would otherwise create an abrupt regime at the end of the zero-stiffness region. The stroke of any conical disk spring from unloaded to fully inverted is twice its height, which requires a minimum spacer height of $2h$ to prevent interference. Second, rigid spacers help maintain concentric alignment of the springs and spacers via a small lip on both the inner and outer spacers. For controlled vertical motion (1DOF) vibration testing, this is sufficient to keep the stack together as long as it remains in compression. For practical applications, a more robust assembly method may be needed to contain the springs. There is a small clearance of about 0.25 mm between the spring outer diameter and outer spacer lip diameter. This allows space for the spring outer diameter to expand slightly as the spring cross section rotates during compression. Similar clearance exists for spring inner diameter and inner spacer lip. Finally, spacer materials and properties determine the edge friction interaction, which is an important aspect of coned disk design as previously discussed. The friction

between the disk spring edges and inner and outer spacers is the primary contributor to damping in the disk spring stack system. Therefore, friction poses both a challenge ("foe") and opportunity ("friend") to tailor the performance, and the spacers offer a convenient way to control the friction by changing spacer material or surface properties.

It is important to note that Eqn. (1) has been previously applied only for deflections up to the flat position[19], but in this work disk springs are compressed past the flat position. Theoretically, before the flat position, the disk spring slides along the horizontal surface of the spacer, and after the flat position, it pivots about the inner corner of the spacer. This change in contact point would result in a sudden decrease in the moment arm length and a corresponding jump in the force as the spring moves through the flat position. Practically, such behavior is not observed due to the small chamfers on disk spring and spacer edges, and the force is distributed over a certain area rather than at a single point. Also, the spacer overlap with the spring is typically very small (<0.5 mm). For these reasons, we assume that Eqn. (1) is a reasonable engineering approximation for the force over the whole deflection range from unloaded to fully inverted states.

Equation (3) can be used to determine the force-deflection curve of a stack with n springs under the assumption that all the springs are equivalent (i.e., they always have the same displacement).

$$\boldsymbol{P\left(\frac{\delta}{n}\right)} = \frac{\frac{E\left(\frac{\delta}{n}\right)\pi}{a^2}\left(\frac{\alpha}{\alpha-1}\right)^2\left[\left(h-\frac{\delta}{n}\right)\left(h-\frac{\delta}{2n}\right)\left(\frac{\alpha+1}{\alpha-1}-\frac{2}{\ln(\alpha)}\right)\tau+\frac{\tau^3}{6}\ln\alpha\right]}{1-\left[\frac{[a\mu_a-b\mu_b-c(\mu_a-\mu_b)](h-\delta)}{(a-b)^2}+\frac{\tau(\mu_a+\mu_b)}{2(a-b)}\right]\text{sgn}(\dot{\delta})} \tag{3}$$

Otherwise, the individual deflections of each spring must be found in order to solve the stack force-deflection relationship. These deflections can be written as the difference of spacer deflections, which are defined in Fig. 3 as $\{\delta_1, \delta_2, \ldots \delta_{n-1}\}$ where n is the number of springs in the stack. Then using Eqn. (1), the forces in each disk spring can be related by:

$$\begin{gathered} P(\delta_{stack} - \delta_{n-1}) = P(\delta_{n-1} - \delta_{n-2}) \\ P(\delta_{n-1} - \delta_{n-2}) = P(\delta_{n-2} - \delta_{n-3}) \\ \vdots \\ P(\delta_2 - \delta_1) = P(\delta_1) \end{gathered} \tag{4}$$

If the stack is under displacement control and the input is δ_{stack}, then the resulting force in the stack can be found by:

$$P_{stack} = P(\,\delta_{stack} - \delta_{n-1}) \tag{5}$$

These n nonlinear algebraic equations can then be solved at each $\delta_{stack}$to determine the unknown variables $\{\delta_1, \delta_2, \ldots \delta_{n-1}, P_{stack}\}$. Due to a large number of nonlinear equations, this system of equations must be solved using numerical methods. Using existing analytical models, the coned disk thickness, inner diameter, and outer diameter can be easily designed to target any QZS force level while keeping stresses below critical values. Briefly, the h/τ should be set to 1.41. Then, the thickness should be set to get to target the approximate QZS force. Next, the inner diameter and outer diameter should be tuned to achieve a target maximum stress. Finally, assuming the static equilibrium point of the mass-isolator system is in the center of the QZS region, the number springs in the stack can be determined by knowledge of the expected vibration amplitudes.

Using the disk spring with geometry in Table 1, we constructed stacks with varying number of springs and measured the force-deflection which is plotted in Fig. 4a. As expected, the working range of the QZS region is extended with increasing number of springs. Also, the QZS property and QZS force are maintained. Eqn. (3) was used to model these stacks, and the results can be seen in Fig. 4b. Overall, good agreement between experiment and model is obtained, although some key differences are noted. The model shows that hysteresis decreases from the beginning to the end of the QZS region. This is not observed experimentally. Secondly, some local areas of negative stiffness within the QZS region can be seen in the experimental results. This is likely caused by some springs having a small snap-through response, indicating that they may have a h/τ ratio greater than 1.41. We expect a certain variation from the nominal ratio of 1.40 exists, and therefore some springs will have some negative stiffness characteristics. Both these differences between experiment and model can be explained by the springs in the stack not being identical. Even small variations in the nominal geometry can lead to substantial differences in deflections between springs in the stack, especially if any springs have h/τ ratio greater than 1.41 which leads to snap-through events. Consequently, Eqn. (3) fails to accurately model the edge friction behavior of the system and cannot predict snap through events because it is simply a linear scaling of Eqn. (1). Equations (4) and (5) are anticipated to more accurately capture all the possible nonlinear behaviors of disk spring stacks because even small spring-to-spring variations can invalidate the primary assumption of Eqn. (3).

Next, in order to estimate the compactness of disk spring stack-based QZS isolators, we perform strain calculations and compare it to typical strain values for QZS isolators based on a linear vertical spring plus negative stiffness disk spring. The full deflection of a single disk spring is two times its height, h, regardless of the other dimensions. Therefore, a minimum spacer height of $2h$ is required to prevent interference of adjacent springs during stack compression (see Fig. 3a). The maximum deflection of the stack is given by:

$$d_s = 2hn \tag{6}$$

where n is the number of springs in the stack. Assuming each spacer has the minimum height, the total height of the stack, H_s is given by Eqn. (7). It should be noted that the height H in this equation is the overall height of each disk spring and is different from the cone height defined in Fig. 1. Here, H can be calculated from h according to Eqn. (8) assuming small angle approximation and height/thickness ratio is 1.41.

$$H_s = Hn + 2h(n+1) \tag{7}$$

$$H = h + \frac{h}{1.41} \tag{8}$$

Now, using Eqns. (6-8), the overall stack strain can be calculated by Eqn. (9).

$$\boldsymbol{\epsilon_s = \frac{d_s}{H_s}} \tag{9}$$

The stack strain is independent of the spring dimensions, and therefore is plotted for an arbitrary spring stack in Fig. 5. It is observed that the strain asymptotically approaches 0.54 or $2\sqrt{2}/(3\sqrt{2}+1)$. The effect of the two end spacers is to lower the strain when n is small but becomes less significant as n increases. Based on estimates from the previous literature, the QZS isolators made from a linear vertical spring plus negative stiffness cone disk have strains in the range of 10-20%[12]. Alternatively, we see that

QZS isolators made from disk spring stacks can achieve strains of 35% for a single disk spring and >50% strain for stacks with at least 7 springs. This is an important advantage that helps to minimize the overall size of the isolator.

Lastly, calculation of strain has included both the top and bottom spacers that each have thickness $2h$. In reality, these spacers only need thickness h because they are adjacent to only one disk spring. Therefore, there is the possibility to further increase the strain, especially at low n.

As we have demonstrated, such conical disk springs and stacked design should have several benefits as QZS isolators including simple construction, low cost, small footprint (Fig. 3b), compressible by up to 54%, and easily customizable to any QZS force. However, some additional practical considerations are needed. The springs and spacers as described in the previous section are simply stacked on top of each other and are not fixed together in any other way. A robust containment method that integrates these parts into a single component is an important design feature. The containment method should have minimal effect on the performance of the QZS isolator. In particular, the important engineering considerations (and challenges) are as follows:

- Does not substantially reduce the overall stack strain: The containment method should not affect the overall strain because compactness is one of the key advantages of disk spring QZS stacks.
- Has minimal effect on the standard stack force-deflection curve: The containment method may introduce some additional vertical stiffness into the system, and this stiffness should not significantly alter the overall QZS behavior.
- Has sufficient lateral strength: The uncontained stack has poor resistance to lateral loads or mixed loading conditions; one of the primary functions of the containment method is to provide strength in directions other than vertical.
- Simple and quick assembly: This requirement is important not only for research purposes to allow quick testing of different configurations and parameters, but also from a production and cost standpoint.
- Tolerant to misalignment: In many applications, the load may not be perfectly centered with the central axis of the stack or may be muti-dimensional; under these types of loading, the containment method should not hinder the function of the stack, which naturally has some ability to compress asymmetrically.

We introduce three new stack containment methods and analyze them with respect to the above-mentioned five engineering requirements. The methods are introduced in Fig. 6(a-c), and are called "tube and shaft design", "retaining spacer design", and "zero Possion's ratio (ZPR) sleeve design" respectively. The concept of the tube and shaft design is to insert the standard stack into a tube as shown in Fig. 6a. A fixed shaft in the center of the tube acts as a linear guide for the piston which is connected to the load and compresses the stack. Horizontal screws at the top of the tube act as a stopper for the piston in a scenario where the assembly may be subject to a tensile load. These screws also act to apply a small preload (1-2 N) to the stack such that the stack will always be in compression. While the outer spacers are centered by the tube, the small preload reduces the possibility for the inner spacers or springs to slip out of concentric alignment. The retaining spacer design in Fig. 6b consists of augmented inner and outer spacers that can hold adjacent disk springs together. Standard inner and outer spacers are modified with

a lip on the top and bottom to contain the disk springs as shown. In order to insert the springs, the retaining spacers must contain a small gap.

Outer and inner retaining spacers can then be either expanded or compressed respectively to enable insertion of the springs. This concept was inspired by conventional snap rings which are installed by a similar technique. The third method (zero Poisson's ratio (ZPR) sleeve) was inspired from work on negative stiffness honeycombs which have a curved beam as the unit cell[21]. We recognized that this geometry may be useful as a sleeve for the isolator stack because it has both zero Poisson's ratio and a snap through regime, making it consistent with disk spring characteristics. We converted the rectangular shape of the honeycomb to a circular one by giving the unit cell a small curvature out of plane and having an integer number of unit cells around the circumference (Fig. 6c). The standard stack is inserted into the sleeve, and then the assembly can be compressed as a whole.

5 EXPERIMENTAL METHODS

5.1 Quasi-Static Tests

Quasi-static force-deflection curves of disk spring stacks are measured on a custom-built setup (Fig. 7) with 500 N Kyowa load cell, Omega LVIT displacement sensor, and motorized linear actuator. Each stack is constructed with 6 disk springs separated by steel inner and outer spacers. A displacement is applied to the top of the top spacer. Control of the linear actuator and data acquisition is done in NI LabView. Full stroke force deflection curves are obtained by compressing the stacks from 0 to 200 N and then reversing back from 200 to 0 N. At 200 N, the disk springs are close to their fully inverted positions. The deflection rate is approximately 0.5 mm/s for all tests. This was determined to be a sufficiently slow rate to avoid any velocity-dependent behavior in the force-deflection curves.

5.2 Vibration Test

The experimental base excitation setup is shown in Fig. 8. The disk spring stack is connected between a mass and electrodynamic shaker. The mass is 10.7 kg and was selected such that the static equilibrium position of the system is approximately in the middle of the QZS region. The mass is guided by 2 linear bearings and shafts, which ensured the force applied to the isolator was purely vertical and aligned to the stack central axis. The electrodynamic shaker (Controlled Vibration Model EDP-1818) is controlled by VibrationView closed loop controller from Vibration Research. The profiles are constant deflection sine sweeps (0.75, 1.0, and 1.25 mm pk-pk) over the frequency range 4-25 Hz with sweep rate of 8 Hz/min. Accelerometers were mounted on the shaker (input) and mass (output), and the time response was recorded with a sampling frequency of 2 kHz. The resulting frequency resolution is approximately 0.01 Hz.

The vibration test results are reported as transmissibility defined as:

$$T = 20\log_{10}\left(\frac{|x_m|}{|x_b|}\right) \tag{10}$$

where x_m is the deflection of the mass and x_b is the deflection of the base.

6 EXPERIMENTAL RESULTS: EVALUATION OF PROPOSED STACK CONTAINMENT METHODS

Containment method 1 (tube and shaft assembly) results in a 30-50% reduction in the maximum possible stack strain for a given number of springs. The overall height of springs and spacers remains the same, but the piston adds substantially to the overall assembly height. It must extend beyond the top of the tube by at least the stack deflection so that the object to be isolated does not interfere with the tube during compression. For example, the strain for a stack of six springs is reduced by 32% from 0.49 to 0.33 due to the height of the piston. Other aspects of the design such as the screws and base may also add to the overall height. The strain of the retaining spacer method is also reduced from that of the standalone stack. The minimum spacer height must be increased to account for the thickness of the lip on the outer and inner retainers. Lip thickness will depend on the retainer material and manufacturing method. For example, a realistic lip thickness for the 3d-printed nylon retaining rings in Fig. 6b is 0.5 mm. The disk spring height is 0.7mm, and therefore the minimum spacer height increases from 1.4 to 2.4 mm. Strain for a stack of six springs is reduced by 28%, from 0.49 to 0.35.

The ZPR sleeve does not require components to extend above the stack or increases in spacer height. However, the curved beam geometry has its own inherent strain limits based on the buckling-type deformation. Maximum deformation of the unit cell is twice the curved beam height. A similar strain analysis can be performed for the ZPR sleeve except without the assumption that the height/thickness ratio of the unit cell is 1.41. If the unit cell features a double beam as in Fig. 6c, we have found that strains of 0.30-0.35 can be realistically achieved without sacrificing the other requirements. However, if the unit cell has a single beam, strains of 0.45-0.50 are feasible. Since the purpose of a double beam is to induce a certain buckling mode to increase the force[21], it may not be necessary in this application. Consequently, the ZPR sleeve, which is mechanically in parallel to the spring stack, will cause only a small decrease of the maximum possible strain of 54%. In summary, the tube and shaft method and retaining spacer method reduce the overall stack strain by significant percentages while the ZPR sleeve can have negligible effect through careful design and selection of number of springs.

Force-deflection curves of the disk spring stack were measured without and with the containment methods, and the measured results are plotted in Fig. 9. Each stack contains 6 disk springs. The tube and shaft concept has minimal effect on the force-deflection curve, maintaining the same QZS force and only slightly increasing the hysteresis. The retaining spacer concept also does not significantly impact the load-deflection behavior. The springs are observed to have a stronger snap-through behavior which may be due to the retainers imposing a small boundary condition opposing the change in diameters of the inner and outer spring edges. The ZPR sleeve increases the overall QZS force from 110 N to 150 N due to the stiffness of the sleeve, which is in parallel with the stack. However, the QZS effect is maintained because the curved beams in the ZPR sleeve also exhibit nonlinear stiffness, creating good synergy with the QZS disk springs. Such behavior can be accounted for in the design, and therefore all the containment methods minimally effect the QZS property in controlled quasi-static testing.

The requirements for lateral strength and tolerance to misalignment are considered together because they typically have a coupled relationship. Lateral strength was evaluated using a simple load test shown in Fig. 10a. Ability to perform well under misalignment is evaluated by vibration testing, but the results are only qualitatively reported here. The lateral strength of the tube and shaft assembly is the highest because lateral force is directly transmitted to the rigid center shaft and linear bearing. However, this rigid 1DOF structure also has a downfall in that the isolator tends to bind if the base motion has any rotational or non-vertical translational component or the isolated object has multiple DOF. Small

misalignment between the isolator axis and the object center of gravity can also lead to a binding problem. Alternatively, the retaining spacer method has the capability to move in more degrees of freedom within a certain range, but has poor lateral stability because the disk springs easily snap out of the retaining spacer grooves upon application of mixed loading conditions. Retaining spacer stiffness can be increased to compensate, but at the cost of increasing difficulty of assembly.

The ZPR sleeve of Fig. 10 is the most interesting with regard to meeting both requirements simultaneously. It can bend as demonstrated in Fig. 10b to accommodate some misalignment or small rotational input but is also a single continuous part. A challenge was to maximize the lateral strength while keeping the vertical stiffness low to minimize the effect on the overall isolator force-deflection curve. ZPR sleeves were 3D printed by multi-jet fusion from Nylon (E = 1.9 GPa). Fig. 10c shows the geometric parameters of the unit cell that were tuned to achieve this goal. In general, the stiffness is reduced by decreasing the thickness, decreasing the height, and increasing the number of unit cells around the circumference. In iteration 1 (Fig. 10d) the stiffness was too high, and thickness of only 0.5 mm caused poor durability. The thickness was increased in iteration 2 to improve durability, and the height was reduced in an effort to lower the stiffness. The stiffness was reduced more substantially in iteration 3 by decreasing the number of units around circumference from 8 to 7 and further reducing the height. The lateral strength of iteration 3 was very low, and the center support width was increased in iteration 4 to compensate. Finally, iteration 4 has low stiffness and a high lateral strength of 122 N. These results are summarized in Fig. 10e.

Assembly of the tube and shaft method and ZPR sleeve method are straightforward and involve simply inserting the standard stack into the appropriate tube or sleeve. Assembly of the retaining spacer concept is more involved because each spring must be individually placed as shown in Fig. 6b. As the stack is built up, it also becomes more difficult to access and compress the inner retainers for spring placement. If the retainers are made from metal, repeated assembly and disassembly of the stack leads to fatigue of the retainers. Lastly, tight tolerances are needed for the disks springs to fit correctly while also allowing the outer and inner retainers to sufficiently expand and compress for assembly. These qualitative but important observations lead to the conclusion that the retaining ring design is the most challenging from an assembly and manufacturing perspective.

Selection of an appropriate containment method will also depend on the application and the relative importance of the various requirements. If the base vibration and mass are expected to move only in the vertical (1DOF) translation along the isolator axis and space is not a constraint, then the tube and shaft method is a suitable option. A more likely scenario is that the vibration input of the base is multi-directional and that the object is supported by multiple isolators. For example, the tube and shaft assembly may not be appropriate for an automotive seat which has a complex vibration response.

Based on these evaluations, we rated each of the containment methods with respect to the engineering requirements in Table 2. Overall, the ZPR sleeve assembly is the most versatile option for many applications by being the most compact, maintaining the isolator compressibility under some misalignments and multi-dimensional motions, and having good lateral strength. Further improvement of this concept including maximizing the lateral strength is possible through finite element analyses and exploring other unit cells besides the curved beam; this is beyond the scope of this article.

7 EXPERIMENTAL RESULTS: VIBRATION TESTING OF DISK SPRING STACK

The vibration test using the setup in Fig. 8 is done for a stack of 6 springs along with a comparable linear compression spring for the sake of comparison. The measured loading and unloading curves for the QZS stack are displayed in Fig. 11. Significant differences between this stack and the stacks in Fig. 4 are seen. The stack of Fig. 11 has more significant negative stiffnesses and snap-through events in the QZS region. Since each stack was constructed with a different random set of springs, these results further highlight the challenge of disk-to-disk variation and limitation of Eqn. (3) as a stack modeling formulation. Outside the QZS region, the effect of disk-to-disk variation is not as prominent because the springs are operating in more linear regimes. In the initial linear region between 0 and 2 mm, the stiffness is approximately 52 N/mm. Therefore, we select a linear compression spring with $k = 52$ N/mm to compare with the QZS isolator in vibration testing.

Vertical motion transmissibility spectra are plotted in Fig. 12. First, the dynamic performance of the QZS isolator compared to linear isolator is significantly better over the whole frequency range. At the linear isolator natural frequency, the transmissibility of the QZS is 40 dB lower compared with the linear isolator. Therefore, we confirm a clear benefit of the disk spring stacks based QZS isolators, even with disk-to-disk variation. As the excitation amplitude increases, some difference in performance of the QZS isolator are seen as a result of the nonlinear amplitude-dependent characteristics. However, due to the large working range of the QZS region, the effect of excitation amplitude on isolation performance is not substantial. A small shift in the resonant frequency as a function of the excitation amplitude is observed; the resonant frequency is 5.6 Hz for 0.75 mm input, 5.3 Hz for 1.0 mm input, and 4.9 Hz for 1.25 mm input. We see from Fig. 11 that the snap-through events lead to some hysteresis that is not caused by edge friction alone. This hysteresis may increase the dynamic stiffness. It is suspected that when the input amplitude increases even further, the dynamic stiffness will go down, and then the QZS effect cannot be established. In conclusion, a QZS isolator based on disc spring stack is found to have several advantages and superior isolation performance while still having significant room for improvement.

8 CONCLUSION

The primary contribution of this article is the design of an innovative isolator stack which includes commercially available disk springs with specific geometry to achieve desired nonlinear force deflection characteristics with a QZS regime and low damping. A quasi-zero stiffness isolator made from a stack of disk springs and spacers is proposed and is shown to have good QZS behavior while being very compact. Three containment methods for the stack are introduced and analyzed in terms of five engineering requirements while overcoming several challenges. Each of the methods has minimal effect on the quasi-zero stiffness effect based on quasi-static testing, but only the ZPR sleeve maintains the high strain of the stack. Furthermore, the ZPR sleeve has good lateral strength while maintaining bending flexibility to adapt to multidirectional vibration. It is anticipated that these containment methods will be an important aspect of disk spring QZS isolator development leading to practical devices. Based on the fundamental static and dynamic responses of the cascaded disks, as reported in this article, they can now be used to develop low-cost and yet compact vibration isolators.

Moving forward, one of the important ways to improve the isolation performance would be to decrease the natural frequency from 5 Hz, therefore extending the isolated frequency range. Throughout our studies, we had found that the two requirements are necessary to reduce the natural frequency: (a)

the stiffness in the QZS region should be exactly zero with minimal error or allowable deviation, and (b) the hysteresis in the QZS region should be minimized. Therefore, we expect that a reduction in the manufacturing tolerances will be essential for improving the isolation performance by having better control over the stiffness and hysteresis in the QZS region. Secondly, although force-deflection hysteresis needs to be minimized, incorporation of viscous damping and structural damping mechanisms might be a useful tool to further optimize the performance without causing an increase in natural frequency.

Future work should focus on a careful study of the variability of disks and the stack assemblies. In addition to serving as a foundation for continued development of disk spring-based QZS isolators, this article should help in identifying areas of improvement for disk spring-based QZS isolators including damping optimization and reducing geometric tolerance. Finally, the experimental work of this paper should motivate future researchers to develop nonlinear computational or semi-analytical solutions for the force-deflection relations over multiple stiffness regimes.

9. CITATIONS

1. C. Liu, K. Yu, B. Liao, and R. Hu, "Enhanced vibration isolation performance of quasi-zero-stiffness isolator by introducing tunable nonlinear inerter", Communications in Nonlinear Science and Numerical Simulation, **95**:105654, 2021.
2. P. Alabuzhev, Vibration protection and measuring systems with quasi-zero stiffness. CRC Press, (1989).
3. K. Ye, J. Ji, and T. Brown, "Design of a quasi-zero stiffness isolation system for supporting different loads", Journal of sound and vibration, **471**:115198, 2020.
4. X. Qu, D. Cao, Q. Wang, and Y. Li, " Design and research of flexible joint with variable stiffness based on torsion spring", in IEEE International Conference on Mechatronics and Automation, (2019), 325–329.
5. G. Gatti, " Statics and dynamics of a nonlinear oscillator with quasi-zero stiffness behaviour for large deflections", Communications in nonlinear science and numerical simulation, **83**:105143, 2020.
6. J. Zhou, Q. Xiao, D. Xu, H. Ouyang, and Y. Li, " A novel quasi-zero- stiffness strut and its applications in six-degree-of-freedom vibration isolation platform", Journal of Sound and Vibration, **394**:59–74, 2017.
7. Y. Jiang, C. Song, C. Ding, and B. Xu, "Design of magnetic- air hybrid quasi-zero stiffness vibration isolation system", Journal of Sound and Vibration, **477**:115346, 2020.
8. J. Zhou, X. Wang, and Y. Mei, "Characteristic analysis of a quasi-zero-stiffness vibration isolator", in IOP Conference Series: Materials Science and Engineering, IOP Publishing, (2 **397**, 0120452018.
9. Y. Buryan, M. Silkov, and A. Zubarev, "Vibration isolation support for processing equipment with quasi-zero stiffness effect on the base of air spring with rubber-cord shell", in AIP Conference Proceedings, AIP Publishing LLC, (2018), **2007**, 030002.
10. A. Carrella, M. Brennan, and T. Waters, " Static analysis of a passive vibration isolator with quasi-zero-stiffness characteristic", Journal of sound and vibration, **301**(3-5):678–689, 2007.
11. T. Le and K. Ahn, " A vibration isolation system in low frequency excitation region using negative stiffness structure for vehicle seat", Journal of Sound and Vibration, **330**(26):6311–6335, 2011.
12. Y. Zhou and P. Chen, "Investigations on a vertical isolation system with quasi-zero stiffness property", Smart Structures and Systems, **25**(5):543–557, 2020.
13. Y. Zhou, P. Chen, and G. Mosqueda, " Analytical and numerical investigation of quasi-zero stiffness vertical isolation system", Journal of Engineering Mechanics, **145**(6):04019035, 2019.
14. L. Meng, J. Sun, and W. Wu, " Theoretical design and characteristics analysis of a quasi-zero stiffness isolator using a disk spring as negative stiffness element", Shock and Vibration, **2015**, 2015.

15. F. Niu, L. Meng, W. Wu, J. Sun, W. Zhang, G. Meng, and Z. Rao, " Design and analysis of a quasi-zero stiffness isolator using a slotted conical disk spring as negative stiffness structure", Journal of Vibroengineering, **16**(4):1769–1785, 2014.
16. A. Valeev, A. Zotov, S. Kharisov, "Application of disk springs for manufacturing vibration isolators with quasi-zero stiffness", Chemical and Petroleum Engineering, **51**:194-200, 2015.
17. A. Valeev, "Dynamics of a group of quasi-zero stiffness vibration isolators with slightly different parameters." Journal of Low Frequency Noise, Vibration and Active Control 37.3 (2018): 640-653.
18. S. Ozaki, K. Tsuda, and J. Tominaga, "Analyses of static and dynamic behavior of coned disk springs: effects of friction boundaries", Thin-Walled Structures, **59**:132–143, 2012.
19. N. Mastricola, J. Dreyer, and R. Singh, " Analytical and experimental characterization of nonlinear coned disk springs with focus on edge friction contribution to force-deflection hysteresis", Mechanical Systems and Signal Processing, **91**:215–232, 2017.
20. J. Almen, and A. Laszlo, "The uniform-section disk spring", Trans. ASME **58**:305–313, 1936.
21. C. Dixon M., C. Seepersad, and M. Haberman. "Mechanical design of negative stiffness honeycomb materials", Integrating Materials and Manufacturing Innovation, **4**:165-175, 2015.

Table 1: Nominal geometry of coned disk spring considered in this paper; see Fig. 1 for the symbols.

Parameter	Nominal value [mm]
a	17.25
b	11.2
h	0.7
τ	0.5

Table 2: Assessment of the three containment methods with respect to the engineering requirements (Rating Key: 1 = Poor, 2 = Unsatisfactory 3 = Average, 4 = Satisfactory, 5 = Very Good)

Three Containment Methods (Figs. 6, 9,10)	Retaining ring method	Tube and shaft method	ZPR (zero Poisson's ratio) sleeve method
Engineering Requirement	**Rating**		
1. Does not substantially reduce overall stack strain	2	2	5
2. Has minimal effect on the standalone stack force-deflection	5	5	4
3. Has sufficient lateral strength	2	5	4
4. Simple and quick assembly	1	4	5
5. Tolerance to misalignment	3	1	5
Rating Sum	**13** (most challenging design)	**17**	**23** (best design)

List of Figure Captions

Fig. 1—Schematic and force-deflections of a typical coned disk spring: Geometry of single disk spring where τ is the thickness, b is the inner radius, a is the outer radius, h is the height, μ_e is the edge friction coefficient, P is the static force, and δ is the static deflection (a), and force-deflection dependence on the h/τ ratio[20](b).

Fig. 2—Effect of the edge friction coefficient on stiffness in the QZS region found using Eqn. (1) in the loading direction: calculated force-deflection curves (a), and calculated stiffness-deflection curves from the derivative of Eqn. (1) (b).

Fig. 3—Geometry, design, and loading of proposed disk spring stack (a), and image of a fabricated disk spring stack containing 6 springs and steel spacers (b).

Fig. 4—Stack force-deflection curves with different number (n) of springs: measured (a) and predicted (with Eqns. (3-4)) assuming a friction coefficient of 0.7 (b).

Fig. 5—Maximum strain for a stack of disk springs (from n = 1 to 10) and corresponding rigid *spacers*, which *have the minimum height of 2h.*

Fig. 6—Overview of three different stack containment methods: tube and shaft design (a), retaining spacer design (b), and zero Poisson's ratio (ZPR) sleeve design (c).

Fig. 7—Experimental setup for measuring quasi-static force-deflection of the QZS stack.

Fig 8—Vibration test setup with shaker table providing base excitation, coned disk stack isolator, rigid block (mass), guide shafts, and sensors.

Fig. 9—Measured force-deflection curves of with 3 containment stack methods (red lines) and comparison with the standard stack (blue line). Tube and shaft containment method (a), retaining spacer containment method (b), and ZPR sleeve containment method (c).

Fig. 10—Lateral strength test of ZPR sleeve (a), demonstration of rotational capability of ZPR sleeve (b), geometric parameters of ZPR unit cell tuned to increase lateral strength (c), summary of ZPR geometry design iterations to increase lateral strength (d), and failure load of ZPR sleeve as a function of design iterations (e).

Fig. 11—Measured force-deflection results of a stack of 6 springs used for amplitude-dependent vibration test.

Fig. 12—Measured motion transmissibility spectra using the spring stack based QZS isolator (of Fig. 11) and comparison with a comparable linear isolator (blue line).

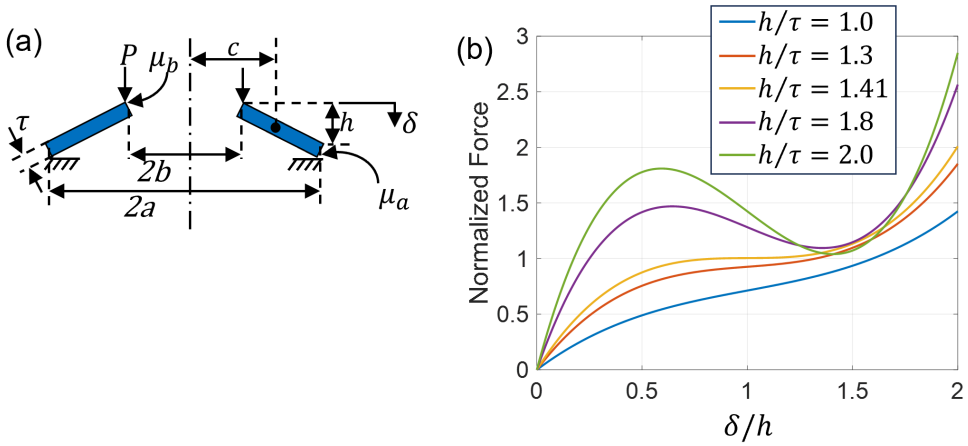

Fig. 2—Schematic and force-deflections of a typical coned disk spring: Geometry of single disk spring where τ is the thickness, b is the inner radius, a is the outer radius, h is the height, μ_e is the edge friction coefficient, P is the static force, and δ is the static deflection (a), and force-deflection dependence on the h/τ ratio[20](b).

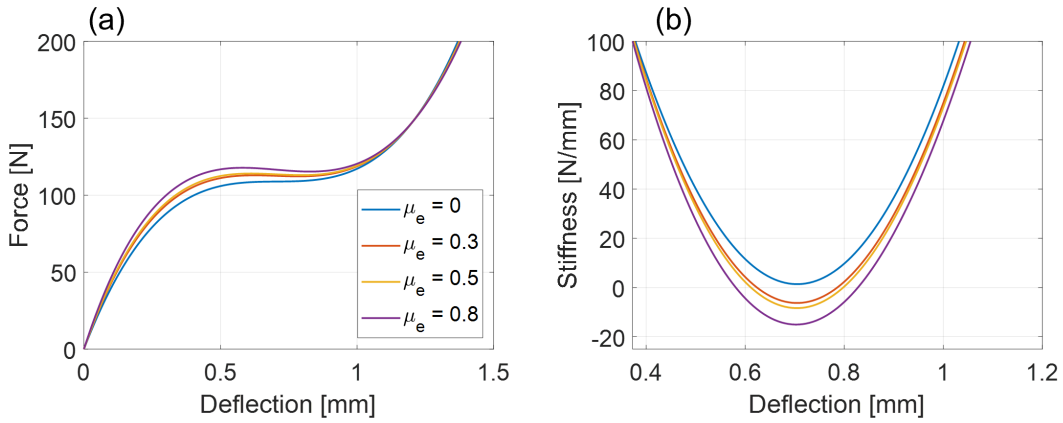

Fig. 2—Effect of the edge friction coefficient on stiffness in the QZS region found using Eqn. (1) in the loading direction: calculated force-deflection curves (a), and calculated stiffness-deflection curves from the derivative of Eqn. (1) (b).

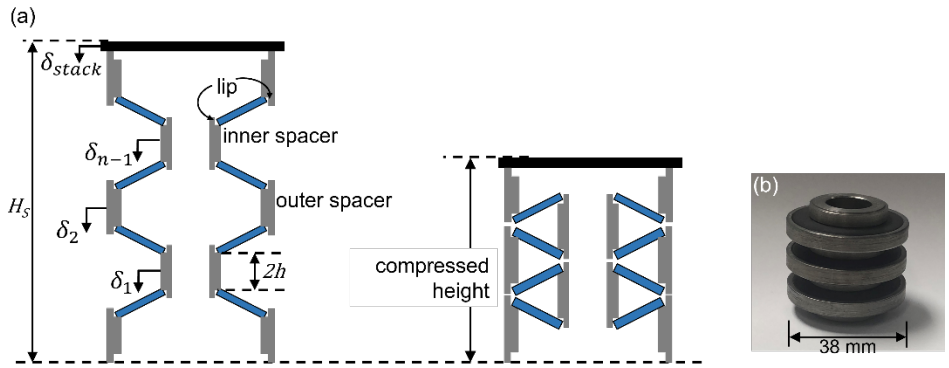

Fig. 3—Geometry, design, and loading of proposed disk spring stack (a), and image of a fabricated disk spring stack containing 6 springs and steel spacers (b).

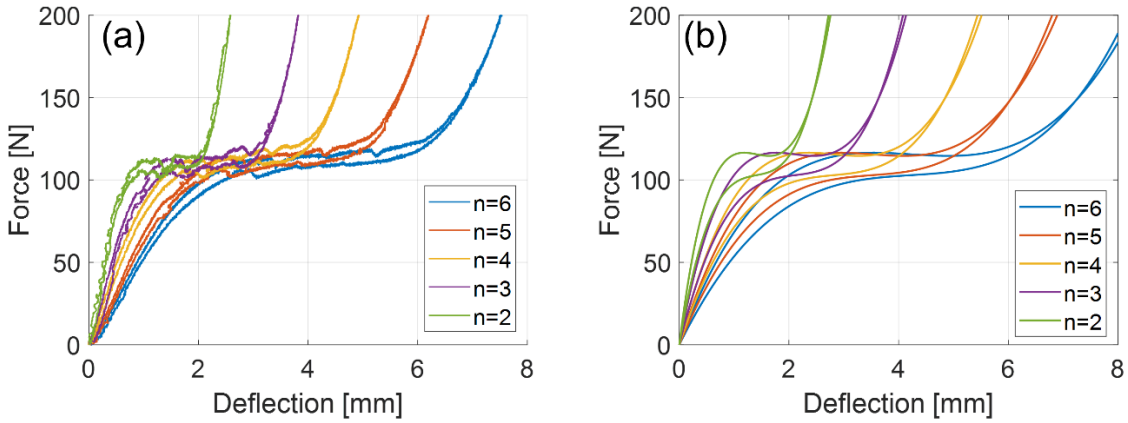

Fig. 4—Stack force-deflection curves with different number (n) of springs: measured (a) and predicted (with Eqns. (3-4)) assuming a friction coefficient of 0.7 (b).

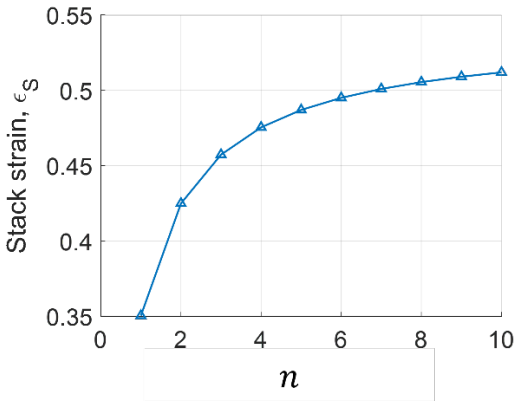

Fig. 5—Maximum strain for a stack of disk springs (from n = 1 to 10) and corresponding rigid *spacers*, which *have the minimum height of 2h.*

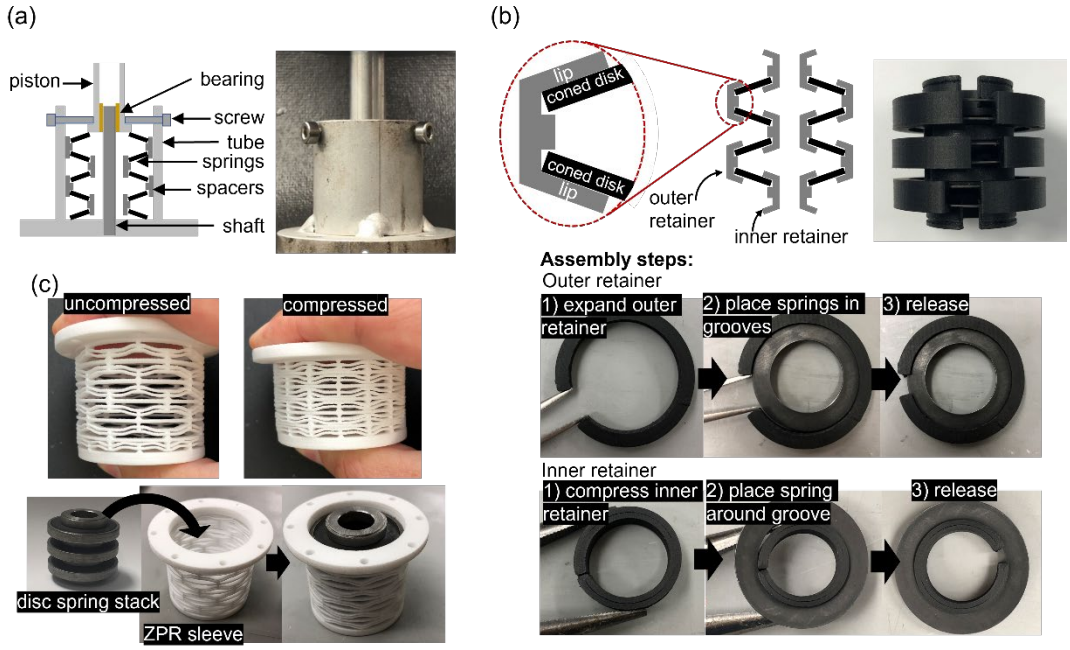

Fig. 6—Overview of three different stack containment methods: tube and shaft design (a), retaining spacer design (b), and zero Poisson's ratio (ZPR) sleeve design (c).

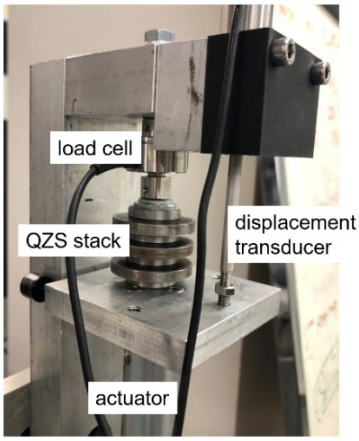

Fig. 7—Experimental setup for measuring quasi-static force-deflection of the QZS stack.

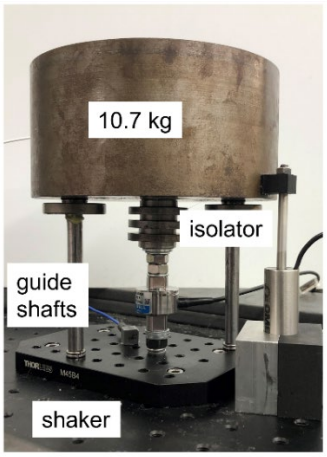

Fig 8—Vibration test setup with shaker table providing base excitation, coned disk stack isolator, rigid block (mass), guide shafts, and sensors.

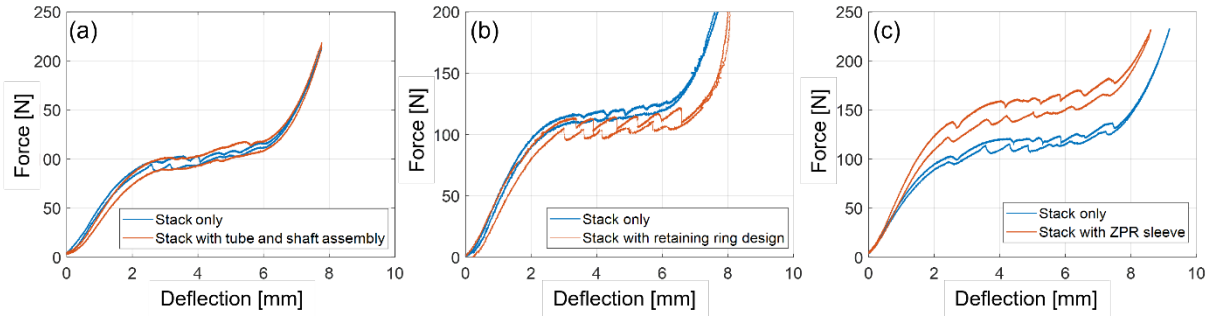

Fig. 9—Measured force-deflection curves of with 3 containment stack methods (red lines) and comparison with the standard stack (blue line). Tube and shaft containment method (a), retaining spacer containment method (b), and ZPR sleeve containment method (c).

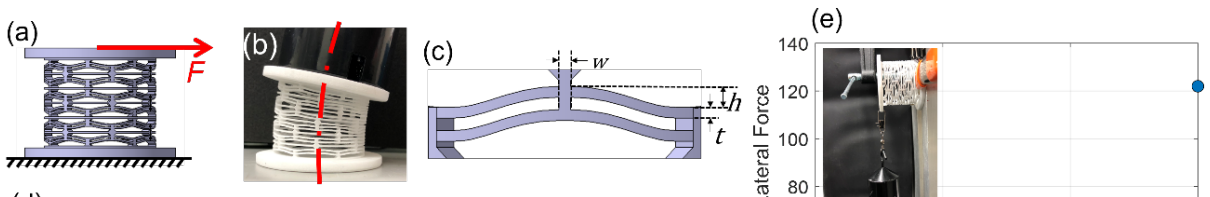

(d)

Iteration #	thickness, t [mm]	height, h [mm]	center support width, w [mm]	unit cells around circumference
1	0.55	1.47	0.75	8
2	0.65	1.25	.75	8
3	0.65	1.0	1.0	7
4	0.65	1.0	1.6	7

Fig. 10—Lateral strength test of ZPR sleeve (a), demonstration of rotational capability of ZPR sleeve (b), geometric parameters of ZPR unit cell tuned to increase lateral strength (c), summary of ZPR geometry design iterations to increase lateral strength (d), and failure load of ZPR sleeve as a function of design iterations (e).

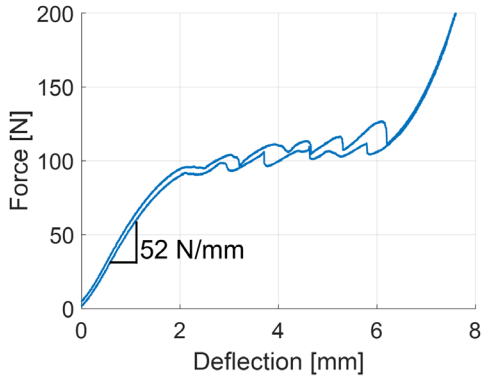

Fig. 11—Measured force-deflection results of a stack of 6 springs used for amplitude-dependent vibration test.

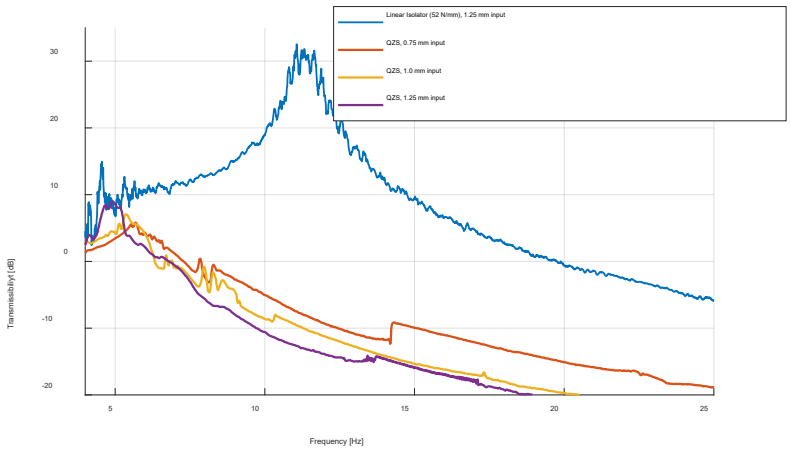

Fig. 12—Measured motion transmissibility spectra using the spring stack based QZS isolator (of Fig. 11) and comparison with a comparable linear isolator (blue line).